Identification of bis-benzylisoquinoline alkaloids as SARS-CoV-2 entry inhibitors from a library of natural products in vitro

Running title: SARS-CoV-2 entry inhibitors

Chang-Long He[1, #], Lu-Yi Huang[1, #], Kai Wang[1, #], Chen-Jian Gu[2], Jie Hu[1], Gui-Ji Zhang[1], Wei Xu[2], You-Hua Xie[2,*], Ni Tang[1,*], Ai-Long Huang[1,*]

[1]Key Laboratory of Molecular Biology for Infectious Diseases (Ministry of Education), Institute for Viral Hepatitis, Department of Infectious Diseases, The Second Affiliated Hospital, Chongqing Medical University, Chongqing, 400010, China

[2]Key Laboratory of Medical Molecular Virology (MOE/NHC/CAMS), Department of Medical Microbiology and Parasitology, School of Basic Medical Sciences, Shanghai Medical College, Fudan University

[#]These authors contributed equally to this work.

***Corresponding authors:**

Ai-Long Huang, **Ni Tang**, Key Laboratory of Molecular Biology for Infectious Diseases (Ministry of Education), Institute for Viral Hepatitis, Department of Infectious Diseases, The Second Affiliated Hospital, Chongqing Medical University, Chongqing, China. Phone: 86-23-68486780, Fax: 86-23-68486780, E-mail: ahuang@cqmu.edu.cn (A.L.H.), nitang@cqmu.edu.cn (N.T.); **You-Hua Xie**, Key Laboratory of Medical Molecular Virology (MOE/NHC/CAMS), School of Basic

Medical Sciences, Shanghai Medical College, Fudan University, e-mail, yhxie@fudan.edu.cn

Abstract

Coronavirus disease 2019 (COVID-19) caused by severe acute respiratory syndrome coronavirus 2 (SARS-CoV-2) is a major public health issue. To screen for antiviral drugs for COVID-19 treatment, we constructed a SARS-CoV-2 spike (S) pseudovirus system using an HIV-1-based lentiviral vector with a luciferase reporter gene to screen 188 small potential antiviral compounds. Using this system, we identified nine compounds, specifically, bis-benzylisoquinoline alkaloids, that potently inhibited SARS-CoV-2 pseudovirus entry, with EC_{50} values of 0.1–10 μM. Mechanistic studies showed that these compounds, reported as calcium channel blockers (CCBs), inhibited Ca^{2+}-mediated membrane fusion and consequently suppressed coronavirus entry. These candidate drugs showed broad-spectrum efficacy against the entry of several coronavirus pseudotypes (SARS-CoV, MERS-CoV, SARS-CoV-2 [S-D614 and S-G614]) in different cell lines (293T, Calu-3, and A549). Antiviral tests using native SARS-CoV-2 in Vero E6 cells confirmed that four of the drugs (SC9/cepharanthine, SC161/hernandezine, SC171, and SC185/neferine) reduced cytopathic effect and supernatant viral RNA load. Among them, cepharanthine showed the strongest anti-SARS-CoV-2 activity. Collectively, this study offers new lead compounds for coronavirus antiviral drug discovery.

Introduction

The novel coronavirus reported in 2019 (2019-nCoV), officially named severe acute respiratory syndrome coronavirus 2 (SARS-CoV-2), is a new type of coronavirus

belonging to the genus *Betacoronavirus*. It is a single-stranded RNA virus with a genome of approximately 29 Kb and with a high pathogenicity and high infectivity.[1-3] As of 8 December 2020, there were nearly 68 million confirmed cases of coronavirus disease 2019 (COVID-19) globally, including more than 1.5 million confirmed deaths, and the number of countries, areas, or territories with cases had reached 220.[4] Although some countries have contained the pandemic, the number of confirmed cases and deaths is expected to rise globally. Currently, no licensed specific antiviral drugs are available to combat the infection. The development of effective viral inhibitors and antibody-based therapeutics for COVID-19 is a high global priority.

The SARS-CoV-2 RNA genome encodes 29 structural and non-structural proteins, including spike (S), envelope (E), membrane (M), nucleocapsid (N) proteins, and the ORF1a/b polyprotein.[5] The S glycoprotein embedded as a trimer in the virus envelope is a key structural protein that mediates SARS-CoV-2 entry into host cells.[6] SARS-CoV-2 S protein comprises two functional subunits, of which S1 is responsible for binding to host-cell receptors and S2 mediates the fusion of viral and cell membranes. Binding of the receptor-binding domain (RBD) located in the S1 subunit of SARS-CoV-2 S protein to the receptor angiotensin converting enzyme 2 (ACE2) is crucial for viral entry into cells.[7-9] Blockade of SARS-CoV-2 entry has become an attractive therapeutic strategy as it prevents the initiation of any steps towards viral replication. To date, antibodies blocking S–ACE2 interaction have proven to be the most effective for COVID-19 treatment.[10-12] However, their high cost limits their broad application. Thus, small molecule-based drugs targeting virus entry steps are

highly anticipated.

Efforts to find SARS-CoV-2 entry inhibitors have led to the identification of several drug candidates. Lipopeptides targeting the HR1 domain in S2 significantly inhibited SARS-CoV-2 entry.[13-15] Host proteases furin, TMPRSS2, and cathepsin B/L help cleave S, thus facilitating the entry process. Inhibition of their activities by small-molecule inhibitors such as camostat or E-64d blocks SARS-CoV-2 infection.[16-18] Apilimod, an inhibitor of the lipid kinase PIKfyve, inhibits viral infection by preventing the release of viral contents from endosomes.[19] Although some progress has been made toward SARS-CoV-2 entry inhibitors, there is still more work to be done.

In this study, we successfully constructed a high-titer SARS-CoV-2 S pseudovirus system using an HIV-1-based lentiviral vector with a luciferase reporter gene for the screening of specific viral entry inhibitors. Based on this classic pseudovirus model, a small potential antiviral compound library was screened. We identified several compounds, especially, bis-benzylisoquinoline alkaloids, that potently inhibited SARS-CoV-2 pseudovirus entry, with EC_{50} values of 0.1–10 μM. Subsequently, we preliminarily explored the underlying mechanisms of the hit compounds, and their antiviral activity against SARS-CoV-2 was confirmed in Vero E6 cells with authentic virus. We identified compounds with effective antiviral activity, thereby providing new lead compounds for coronavirus antiviral drug discovery.

Results

Screening of SARS-CoV-2 S-G614 entry inhibitors in 293T-ACE2 cells

The S protein variant D614G (a single change in the genetic code; D = aspartic acid, G = glycine) carrying the amino acid mutation D614G has become the most prevalent form in the global pandemic and has been associated with increased infectivity of SARS-CoV-2.[20-22] Using a luciferase-expressing pseudovirus encoding SARS-CoV-2 S (G614) protein, a library of 188 chemical compounds (Supplementary Table S1, most were natural compounds) was screened in 293T-ACE2 cells to find novel anti-SARS-CoV-2 entry inhibitors. A workflow chart of screening is shown in Fig. 1a. 293T-ACE2 cells were pretreated with 20 μM of each compound for 1 h and then, a SARS-CoV-2 S-G614 pseudovirus (3.8×10^4 copies) mixture containing 20 μM of each compound was added to the cells. A known entry inhibitor, E-64d (targeting host cathepsin B/L), was used as a positive control and DMSO as a negative control. Luciferase activity was measured to assess the inhibitory effect of the 188 compounds on S-G614 pseudovirus entry 72 h post-infection. After a preliminary screening, 41 compounds associated with a relative infection rate <30% (Fig. 1b) were identified. Half of these displayed cytotoxicity at 20 μM. We selected 19 compounds with low cytotoxicity for further testing. The chemical structures of the 19 compounds are shown in Supplementary Fig. S1. The selectivity index values in terms of cytotoxicity were greater than 2, suggesting that they may be safe *in vivo*. As the S-G614 pseudovirus was generated in the envelope-defective HIV-1 backbone, vesicular stomatitis virus (VSV) pseudovirus was used as a control to exclude compounds that have anti-HIV activities. Through a filtering strategy, we identified nine compounds

(SC9, SC161, SC171, SC182, SC183, SC184, SC185, SC186, and SC187) that specifically inhibited S-G614 pseudovirus entry. Except SC171, all these compounds were bis-benzylisoquinoline alkaloids. The EC_{50} values of the nine compounds against S-G614 pseudovirus were below 10 μM, but above 20 μM in VSV-G pseudovirus (Table 1, Supplementary Fig. S2).

Investigation of the treatment timing and antiviral efficacy in different cell lines

Next, we analyzed the relationship between the antiviral efficacy of the nine selected compounds against S-G614 pseudovirus and the timing of treatment. We divided the S-G614 pseudovirus entry into three stages: pretreatment, pseudovirus entry, and pseudovirus post-entry. In total, nine experimental groups were set up for each compound, including eight treatment groups (A–G) and a control group (Fig. 2a). Importantly, pretreatment with each compound (group B in Fig. 2) significantly inhibited S-G614 pseudovirus infection. In the pseudovirus entry stage (group C in Fig. 2), the compounds exerted similar suppressive effects. However, in the pseudovirus post-entry stage (group D in Fig. 2), none of the compounds showed any inhibitory effect. These results indicated that all nine candidates blocked pseudovirus infection by targeting host factors at the entry stage.

Hoffmann *et al*. highlight that cell lines mimicking important aspects of respiratory epithelial cells should be used when analyzing the anti-SARS-CoV-2 activity.[23] Hence, we determined their EC_{50} values against S-G614 pseudovirus in Calu3, A549, and 293T-ACE2 cells (Fig. 3a–i). As shown in Fig. 3, the EC_{50} values of

SC9 (Fig. 3a), SC161 (Fig. 3b), SC171 (Fig. 3c), SC182 (Fig. 3d), and SC185 (Fig. 3g) were below 5 μM in all three cell lines. Unfortunately, the EC_{50} values of SC183 (Fig. 3e), SC184 (Fig. 3f), SC186 (Fig. 3h), and SC187 (Fig. 3i) did not reach the threshold we had set and thus were excluded from subsequent experiments.

Inhibition of entry of pseudovirus bearing coronavirus S protein by the candidate compounds

Considering that SARS-CoV-2, SARS-CoV, and MERS-CoV all belong to the genus *Betacoronavirus*, we next determined whether the remaining compounds have broad-spectrum antiviral effects against these coronaviruses, using pseudovirus-based inhibition assays. We constructed S-D614, S-SARS, and S-MERS pseudoviruses using the same lentiviral system as S-G614, and then determined the EC_{50} values of SC9 (cepharanthine, Fig. 4a), SC161 (hernandezine, Fig. 4b), SC171 (Fig. 4c), SC182 (tetrandrine, Fig. 4d), and SC185 (neferine, Fig. 4e) against these pseudoviruses in 293T cells expressing ACE2 or DPP4. Interestingly, SC9, SC161, SC171, and SC185 exhibited highly potent pan-inhibitory activity against coronavirus S-pseudotyped viruses. The EC_{50} values of the five compounds are shown in Fig. 4f. As SARS-CoV and SARS-CoV-2 have been reported to enter host cells via binding to ACE2, and while DPP4 is critical for MERS-CoV entry, it could be ruled out that the five compounds interfere with ACE2 to block pseudovirus entry.

Interaction between the target compounds and the SARS-CoV-2 RBD domain

Next, we used competitive ELISAs and thermal shift assays to determine whether these five compounds interact with the SARS-CoV-2 RBD domain. SBP1, one of the recombinant ACE2 polypeptides, exhibited a weak ability to inhibit the entry of S-G614 pseudovirus and a weak RBD-binding ability (Fig. 5a, 5b), whereas the interaction between SC9, SC161, SC171, or SC185 and RBD was negligible (Fig. 5b). Thermal shift assay results showed that the ΔT_M values of SC161, SC185, and SBP1 were 0 °C, 0.6 °C, and 1.3 °C, respectively (Fig. 5c–d), indicating that SC161 and SC185 could not stabilize the RBD domain. Thus, the blockade of virus entry by these candidate compounds is not related to interaction with the SARS-CoV-2 RBD domain.

Depletion of Ca^{2+} blocks the entry of SARS-CoV-2 S-G614 pseudovirus

Our data indicated that the above five compounds may target host cells to inhibit SARS-CoV-2 entry. Therefore, we explored host factors via which these five compounds inhibit virus entry in 293T-ACE2 cells. We examined whether these compounds perturb cell fusion mediated by SARS-CoV-2 S protein, the initiation process for virus entry. Compared to DMSO, SC9, SC161, SC182, and SC185 at 5 μM potently inhibited SARS-CoV-2 S-mediated membrane fusion of 293T cells, and the cell-cell fusion rate in the SC171 treatment group was 40% (Fig. 6a, 6b). Previous studies have shown that the calcium ion (Ca^{2+}) plays a critical role in SARS-CoV or MERS-CoV S-mediated fusion to host cell entry.[24,25] Supplementation of the culture medium with 2 mM $CaCl_2$ enhanced S-G614 pseudovirus entry ability by 2-fold

compared with calcium-free medium (Fig. 6c). In contrast, the entry-blocking effect of the compounds sharply decreased in calcium-depleted medium (Fig. 6d–e). Moreover, treatment with 20 μM of BAPTA-AM, a calcium-chelating agent used to deplete intracellular Ca^{2+}, significantly decreased the entry capacity of S-G614 pseudovirus by 70% (Fig. 6f and 6g). More importantly, when cells were pretreated with 20 μM BAPTA-AM in combination with one of the four compounds, among which three bi-benzylisoquinoline alkaloids have been reported as calcium channel blockers (CCBs),[26-30] the EC_{50} values of these compounds against S-G614 pseudovirus decreased by more than 10-fold (Fig. 6h–i). Intracellular cholesterol levels increase upon CCB treatment,[31,32] and upregulation of cholesterol biosynthesis results in blockade of SARS-CoV-2 infection.[33] Consistent herewith, intracellular cholesterol levels increased in 293T-ACE2 cells pretreated with 5 μM SC9, SC161, SC171, and SC185 (Fig. 6j). These data indicated that blockade of S-G614 pseudovirus entry by SC9, SC161, SC171, and SC185 mainly depends on calcium homeostasis.

Cell entry inhibition by the compounds in authentic SARS-CoV-2 infected Vero E6 cells

The antiviral activities of SC9, SC161, SC171, and SC185 were confirmed in Vero E6 cells infected with native SARS-CoV-2. Changes in cell structure and morphology caused by SARS-CoV-2 were observed 48 h post-infection. As shown in Fig. 7a, remdesivir (5 μM), used as a positive control, completely inhibited

SARS-CoV-2-induced cytopathogenic effect (CPE) on Vero E6 cells. SC161 (hernandezine), SC171, and SC185 (neferine) partly inhibited CPE at 10 μM, whereas SC9 (cepharanthine) completely inhibited CPE at 10 μM. Cell supernatants were collected at 48 h post-infection for RT-qPCR quantification of SARS-CoV-2 genomic RNA. The RNA level in the remdesivir (5 μM) treatment group was 0.01% of that in the DMSO control group (Fig. 7b). The RNA levels in the 10 μM SC9, SC161, SC171, and SC185 treatment groups were 0.08%, 70.27%, 43.55%, and 76.98%, respectively, of that in the DMSO control group (Fig. 7c). The results showed that these compounds inhibited SARS-CoV-2 to varying degrees and may be useful as leads for SARS-CoV-2 therapeutic drug development.

Discussion

Viral entry into host cells is one of the most critical steps in the life cycle of a virus. Since blockade of the entry process is a promising therapeutic option for COVID-19, research attention has been focused on the discovery of viral entry inhibitors. To block the entry of SARS-CoV-2, the RBD–ACE2 interaction or viral fusion must be abrogated. To date, a few entry inhibitors against SARS-CoV-2 have been reported.[19,34-37] ACE2 is the key host receptor mediating SARS-CoV-2 entry. Host factors including HMGB1 (an ACE2 expression regulator), calcium channel, and vacuolar ATPases have also been reported to contribute to the infectivity of SARS-CoV-2.[33,38,39] Pharmacological inhibition of these crucial host factors provides another potential therapeutic approach. Although entry SARS-CoV-2 inhibitor development is very attractive, no candidates have progressed into clinical trials.

To address this need, we screened 188 compounds to identify SARS-CoV-2 (S-G614) entry inhibitors in 293T-ACE2 cells. Nineteen compounds, including 11 bis-benzylisoquinoline alkaloids (SC9, SC161, SC180-188) and an analog of VE607 (SC171) were identified. VE607, previously reported as a SARS entry inhibitor with an IC_{50} of 3 μM,[40] did not block SARS-CoV-2 entry at 20 μM in our assay. Among the 19 hits, nine compounds (SC9, SC161, SC171, SC182–187) with relatively high activity, low cytotoxicity, and good specificity were selected for subsequent analyses.

The efficacy of the nine compounds in different SARS-CoV-2 entry stages was examined to clarify whether they interfere with S-ACE2 interaction by targeting S or host factors. The compounds showed effective entry blockade only in the pretreatment stage, and did not bind to the S RBD, indicating that they target host factors. SARS-CoV-2 enters TMPRSS2-negative 293T-ACE2 cells via endocytosis, and TMPRSS2 inhibitors do not block SARS-CoV-2 infection in this cell line.[17] Besides in 293T cells, our hits also inhibited SARS-CoV-2 infection in the TMPRSS2-positive lung epithelial cell lines Calu-3 and A549, indicating that they do not target TMPRSS2.

ACE2 is the common host receptor of SARS-CoV-2 and SARS-CoV, whereas MERS-CoV infection relies on DPP4.[41,42] Interestingly, our findings demonstrated that bis-benzylisoquinoline alkaloids (SC9/cepharanthine, SC161/hernandezine, SC182/tetrandrine, and SC185/neferine) and the VE607 analog SC171 could potently block infection by SARS-CoV-2, SARS-CoV, and MERS-CoV pseudoviruses. Therefore, our compounds do not target ACE2 or DPP4 and thus may target some

other host factors. Recent studies have demonstrated a crucial role of Ca^{2+} in viral fusion of Ebola, SARS-CoV, and MERS-CoV. Ca^{2+} coordinates with negatively charged residues, such as aspartic acid and glutamic acid, within the viral fusion peptide. Depletion of extracellular or especially, intracellular Ca^{2+} significantly reduced infection by these viruses.[24,25,43-45] We noted that the identified bis-benzylisoquinoline alkaloids had been reported as CCBs[26-29]. CCBs, originally used to treat cardiovascular diseases, are supposed to have a high potential to treat SARS-CoV-2 infections[46]. In this study, the bis-benzylisoquinoline CCBs abolished S–ACE2-mediated membrane fusion in 293T-ACE2 cells. Calcium-free medium or intracellular Ca^{2+} chelation significantly diminished SARS-CoV-2 pseudovirus infection, suggesting that Ca^{2+} is required for SARS-CoV-2 entry. Upon pretreatment with BAPTA-AM, the bis-benzylisoquinoline CCBs had >10-fold higher EC_{50} values than those without BAPTA-AM pretreatment. These results corroborated that the efficacy of these inhibitors depends on cellular calcium homeostasis. Additionally, upregulation of cholesterol biosynthesis has been revealed as a common mechanism underlying viral resistance. Perturbation of the cholesterol biosynthesis pathway with the CCB amlodipine reduced viral infection[33]. Consistent herewith, the bis-benzylisoquinoline CCBs upregulated intracellular cholesterol, which likely contributes to infection inhibition.

In conclusion, we reported a set of bis-benzylisoquinoline alkaloids as coronavirus entry inhibitors. These inhibitors effectively protected different cell lines (293T, Calu-3, and A549) from infection by different coronaviruses (SARS-CoV,

MERS-CoV, SARS-CoV-2 [S-D614 and S-G614]) *in vitro*. The compounds block host calcium channels, thus inhibiting Ca^{2+}-mediated fusion and suppressing virus entry. Considering the effectiveness of CCBs in the control of hypertension, our study provided clues to support that CCBs may be useful in treating coronavirus infection in patients with hypertension.

Acknowledgments

We would like to thank Prof. Cheguo Cai (Wuhan University, Wuhan, China) for providing the pNL4-3.Luc.R-E- plasmid. This work was supported by the Key Laboratory of Infectious Diseases, CQMU, 202001, the Science and Technology Research Program of Chongqing Municipal Education Commission (KJQN202000418 to L-Y.H.), Emergency Project from the Science & Technology Commission of Chongqing (cstc2020jscx-fyzx0053 to A-L.H.), the Emergency Project for Novel Coronavirus Pneumonia from the Chongqing Medical University (CQMUNCP0302 to K.W.), the Leading Talent Program of CQ CSTC (CSTCCXLJRC201719 to N.T.), and a Major National Science & Technology Program grant (2017ZX10202203 to A-L.H.) from the Science & Technology Commission of China.

Author contributions

A.L.H., N.T., and Y.H.X. and designed and directed the study. C.L.H., L.Y.H., K.W., J.H., and G.J.Z. constructed the pesudoviruses and screened the compounds. C.J.G. and W.X. performed authentic SARS-CoV-2 assays. All authors reviewed the manuscript and consented to the description of author contribution.

Competing interests: The authors declare no competing interests.

Materials and Methods

Plasmids

The codon-optimized gene encoding SARS-CoV-2 spike (S) protein (GenBank: QHD43416) with 19 amino acids deletion at the C-terminal was synthesized by Sino Biological Inc (Beijing, China), and cloned it into the pCMV3 vector between the restriction enzyme *Kpn*I and *Xba*I sites (denoted as pS-D614). The recombinant plasmid pS-D614 was used as template, and the D614G mutant S-expressing plasmid (denoted as pS-G614) was constructed by site-directed mutagenesis. SARS-CoV S-expressing plasmid (Cat: VG40150-ACGLN, named as pS-SARS) and MERS-CoV S-expressing plasmid (Cat: VG40069-CF, named as pS-MERS) were obtained from Sino Biological Inc (Beijing, China). The VSV-G-expressing plasmid pMD2.G was donated by Prof. Ding Xue from Tsinghua University (Beijing, China). The HIV-1 NL4-3 ΔEnv Vpr luciferase reporter vector (pNL4-3.Luc.R-E-) constructed by N. Landau was donated by Prof. Cheguo Cai from Wuhan University (Wuhan, China). Human ACE2 and DPP4 expression plasmids were derived from GeneCopoeia (Guangzhou, China).

Cell lines and cell culture

HEK 293T, A549, and Calu3 cells were purchased from the American Type Culture Collection (ATCC, Manassas, VA, USA). Cells were cultured at 37 ºC and 5% CO_2 atmosphere in Dulbecco's modified Eagle medium (DMEM; Hyclone, Waltham, MA, USA) containing 10% fetal bovine serum (FBS; Gibco, Rockville, MD, USA), 100

mg/mL of streptomycin, and 100 units/mL of penicillin. HEK 293T cells transfected with human ACE2 and DPP4 (293T-ACE2, 293T-DPP4) were cultured under the same conditions with the addition of G418 (0.5 mg/mL) to the medium.

Antigens and antibodies

The RBD domain of SARS-CoV-2 S protein (His-tag) were synthesized by Prof. Xuefei Cai at Key Laboratory of Molecular Biology for Infectious Diseases (Ministry of Education), Chongqing Medical University. The anti-RBD monoclonal antibody was kindly provided by Prof. Aishun Jin from Chongqing Medical University. RBD-binding peptide SBP1 derived from human ACE2 α helix 1 (IEEQAKTFLDKFNHEAEDLFYQS) was synthesized by GenScript (Nanjing, China).

Compounds and reagents

Custom compound library containing 188 small molecules, remdesivir, and aloxistatin (E-64d) were purchased from MedChemExpress (HY-L027) and Chemdiv. BAPTA-AM (T6245) was purchased from TargetMol. All the compounds were dissolved in dimethyl sulfoxide (DMSO) at a stock concentration of 20 mM.

Cell cytotoxicity assay

The CellTiter 96® AQ_{ueous} One Solution Cell Proliferation Assay (G3582, Promega, USA) was used to assess cell viability according to the product's description. Briefly,

HEK 293T cells were dispensed into 96-well plate ($2x10^4$ cells/well), cultured in medium containing gradient concentrations of the compound for 72 hours at 37 ºC in a humidified 5% CO_2 incubator. The cells were incubated with 100 µl fresh medium after removal of the medium. Then 20 µl of CellTiter 96® AQueous One Solution Reagent was added into each sample well and incubating the plate was incubated at 37°C for 1-4 hours in a humidified 5% CO_2 atmosphere. The absorbance at 490 nm was measured using a microplate reader (Synergy H1, BioTek, USA).

Pseudoviruse production and quantification

Pseudotyped viruses were produced as previously described[47]. Briefly, 5×10^6 HEK 293T cells were co-transfected with 6 µg each of pNL4-3.Luc.R-E- and recombinant plasmid (pS-SARS, pS-MERS, pS-D614, or pS-G614) using Lipofectamine 3000 Transfection Reagent (Invitrogen, Rockville, MD) according to the manufacturer's instructions. After 48 h transfection, pseudotyped viruses expressing S-SARS, S-MERS, S-D614, and S-G614 spike protein were harvested, centrifuged and filtered through 0.45 µm filters, and subsequently stored at -80°C. 293T cells were co-transfected with pNL4-3.Luc.R-E- and pMD2.G plasmid to collect the VSV-G pseudovirus.

The copies of the pseudovirus were expressed as numbers of viral RNA genomes per mL of viral stock solution and determined using RT-qPCR with primers and a probe that targeting LTR. Sense primer: 5′-TGTGTGCCCGTCTGTTGTGT-3′, anti-sense primer: 5′-GAGTCCTGCGTCGAGAGAGC-3′, probe:

5′-FAM-CAGTGGCGCCCGAACAGGGA-BHQ1-3′. Briefly, viral RNAs were extracted according to the manufacturer's instructions with TRIzol reagent (Invitrogen). Then, the TaqMan One-Step RT-PCR Master Mix Reagents (Applied Biosystems, Thermo Fisher) was used to amplify total RNAs. pNL4-3.Luc.R-E- vector with certain copies was used to generate standard curves. All the pseudotyped viruses were titrated to the uniform titer (copies/mL) for the following research.

Compound screening

For pseudovirus-based inhibition assay, 188 compounds were screened via luciferase activity. HEK 293T cells cultured in 96-well plate ($2x10^4$ cells/well) were incubated with each compound (20 μM) for 1 hour and were infected with the same amount of pseudovirus (3.8×10^4 copies in 50 μL). The cells were replaced to fresh DMEM medium 8 h post-infection. Cells were lysed by 30 μl lysis buffer (Promega, Madison, WI, USA) at 72 h post-infection to measure RLU with luciferase assay reagent (Promega, Madison, WI, USA) according to the product description. All data were performed at least three times and expressed as means ± standard deviations (SDs).

Cell-cell fusion assay

HEK 293T effector cells were transfected with plasmid pAdTrack-TO4-GFP encoding green fluorescent protein (GFP) or pS-G614 encoding the corresponding SARS-CoV-2 S protein. 293T-ACE2 cells were used as target cells. At 8 h post-transfection, the effector cells were washed twice with PBS and were pretreated

with compounds or DMSO as control for another 16h. Subsequently, the effector cells were overlaid on target cells at a ratio of approximately one S-expressing cell to two receptor-expressing cells with about 90% confluent. After a 4-hour coculture, images of syncytia were captured with an inverted fluorescence microscope (Nikon eclipse Ti, Melville, NY).

For quantification of cell-cell fusion, three fields were randomly selected in each well to count the fused and unfused cells. The fused cells were at least twice as large as the unfused cells, and the fluorescence intensity was weaker in fused cells since GFP diffusion from one effector cell to target cells. The percentage of cell-cell fusion was calculated as: [(number of the fused cells/number of the total cells) × 100%].

Competitive ELISA

The recombinant RBD proteins derived from SARS-CoV-2 were coated on 96-well microtiter plate (50ng/well) at 4°C overnight. After blocked with blocking buffer (5% FBS and 2% BSA in PBS) for 1 hour at 37°C, serial dilution solutions of compounds, ACE2 peptide SBP1 or DMSO were added into the plates and incubated at 37°C for 1 hour. Plates were washed five times with phosphate-buffered saline, 0.05% Tween-20 (PBST) to remove the free drug or DMSO. The wells were incubated with mouse anti-RBD monoclonal antibody (1:1000 dilution) for 1 hour at 37°C, and then washed with PBST five times and incubated with Horseradish peroxidase (HRP)-conjugated goat anti-mouse antibody (Abmart, Shanghai, China) for 1 hour at 37°C. TMB substrate was added and incubated for 15 minutes at 37°C for color development,

finally the absorbance at 450 nm was measured by a microplate reader.

Differential scanning fluorimetry

Briefly, purified His-RBD was diluted to 200 μg/mL in PBS buffer containing Sypro Orange 5× (ThermoFisher) in a 96-well white PCR plate. Compounds and ACE2 derived peptide SBP1 were added at a final concentration of 20 μM. All samples were tested in triplicate with a Bio-Rad RT-PCR system. The samples were first equilibrated at 25 °C for 3 min, then heated from 25 °C to 85 °C with a step of 1 °C per 1 min, and the fluorescence signals were continuously collected using CFX Maestro. T_m values were calculated as previously described[48].

Functional analysis of Ca^{2+} in pseudovirus infectivity

293T-ACE2 cells were seeded in 96-well plate ($2x10^4$ cells/well) and incubated at 37 °C for 8h. For extracellular calcium depletion assays, cells were washed three times using PBS with or without Ca^{2+}. Calcium-free medium with or without 2 mM calcium chloride and 5 μM compounds were added and incubated for 1h at 37°C. Next, S-G614 pseudovirus was added to the cells for 8 h at 37°C. For intracellular calcium depletion assays, cells were washed three times using PBS with or without Ca^{2+}, DMEM with BAPTA-AM (20 μM) or DMSO and gradient concentrations of compounds were added and incubated for 2 h at 37°C. In the following, S-G614 pseudovirus was added to infect the cells for 8 h at 37°C. For both types of assays, complete medium was then added after removed the medium. The cells were

measured by luciferase activity.

Cellular cholesterol measurement

Cellular cholesterol was measured using the Cholesterol/Cholesterol Ester-Glo™ Assay (J3190, Promega, USA) according to the product's description. In short, HEK 293T-ACE2 cells were assigned to 96-well plates ($4x10^4$ cells/well) and cultured for 24 hours at 37 °C with 5 μM compounds. DMSO was used as negative control. The medium in the 96-well plate was removed and cells was washed twice with 200 μl PBS. Then, 50 μl of cholesterol lysis solution was added, shaking the plate carefully and incubating for 30 minutes at 37°C. Following, 50 μl of cholesterol detection reagent was added with esterase or without esterase to all wells and the plate was incubated at room temperature for 1 hour. Finally, recording luminescence with a plate-reading luminometer. Total cholesterol concentration was calculated by comparing the luminescence of samples and controls under the same condition.

Cytopathic effect (CPE) assay and quantification of SARS-CoV-2 infection

Vero E6 cells were dispensed into 96-well plate ($4.0x10^4$ cells/well), pre-treated with medium containing compounds or DMSO for 1 hour at 37 ºC. Then 60 μl DMEM medium which supplemented with compounds or DMSO was replaced immediately, the same amount of SARS-CoV-2 (100 $TCID_{50}$/well) was added and incubated for 1 hour at 37 ºC. The mixture was removed and the cells were washed twice with PBS, and cultured with 100 μl fresh medium for 48 hours at 37 ºC with 5% CO_2

atmosphere. Cytopathic effects (CPE) induced by the virus was observed using microscope at 48 h post-inoculation. Cell culture supernatant was collected at 48 h post-infection for viral RNA quantification using the novel coronavirus real-time RT-PCR Kit (Shanghai ZJ Bio-Tech Co, Ltd, Shanghai, China). Remdesivir (5 μM) was used as positive control in the experiment.

Statistical analyses

Data were analyzed using GraphPad Prism version 6.0 software and were presented as means ± SD. Statistical significance was determined using ANOVA for multiple comparisons. Student's t test was applied to compare the two groups. Differences with P values < 0.05 were deemed statistically significant.

Data availability

Data supporting the results of this study can be obtained from the author upon request

465

References

1 Coronaviridae Study Group of the International Committee on Taxonomy of, V. The species Severe acute respiratory syndrome-related coronavirus: classifying 2019-nCoV and naming it SARS-CoV-2. *Nat Microbiol* **5**, 536-544 (2020).

2 Liu, Y. *et al.* Aerodynamic analysis of SARS-CoV-2 in two Wuhan hospitals. *Nature* **582**, 557-560 (2020).

3 Zhou, P. *et al.* A pneumonia outbreak associated with a new coronavirus of probable bat origin. *Nature* **579**, 270-273 (2020).

4 Organization, W. H. *Coronavirus disease (COVID-19) situation reports*, <https://www.who.int/emergencies/diseases/novel-coronavirus-2019> (2020).

5 Wang, K. *et al.* Longitudinal dynamics of the neutralizing antibody response to SARS-CoV-2 infection. *Clin Infect Dis* (2020).

6 Wrapp, D. *et al.* Cryo-EM structure of the 2019-nCoV spike in the prefusion conformation. *Science* **367**, 1260-1263 (2020).

7 Yan, R. *et al.* Structural basis for the recognition of SARS-CoV-2 by full-length human ACE2. *Science* **367**, 1444-1448 (2020).

8 Lan, J. *et al.* Structure of the SARS-CoV-2 spike receptor-binding domain bound to the ACE2 receptor. *Nature* **581**, 215-220 (2020).

9 Shang, J. *et al.* Structural basis of receptor recognition by SARS-CoV-2. *Nature* **581**, 221-224 (2020).

10 Cao, Y. *et al.* Potent neutralizing antibodies against SARS-CoV-2 identified by

high-throughput single-cell sequencing of convalescent patients' B cells. *Cell* (2020).

11 Du, S. *et al*. Structurally Resolved SARS-CoV-2 Antibody Shows High Efficacy in Severely Infected Hamsters and Provides a Potent Cocktail Pairing Strategy. *Cell* (2020).

12 Wan, J. *et al*. Human-IgG-Neutralizing Monoclonal Antibodies Block the SARS-CoV-2 Infection. *Cell Rep* **32**, 107918 (2020).

13 Zhu, Y., Yu, D., Yan, H., Chong, H. & He, Y. Design of potent membrane fusion inhibitors against SARS-CoV-2, an emerging coronavirus with high fusogenic activity. *J Virol* (2020).

14 Xia, S. *et al.* Fusion mechanism of 2019-nCoV and fusion inhibitors targeting HR1 domain in spike protein. *Cell Mol Immunol* (2020).

15 Xia, S. *et al.* Inhibition of SARS-CoV-2 (previously 2019-nCoV) infection by a highly potent pan-coronavirus fusion inhibitor targeting its spike protein that harbors a high capacity to mediate membrane fusion. *Cell Res* **30**, 343-355 (2020).

16 Hoffmann, M. *et al*. Nafamostat Mesylate Blocks Activation of SARS-CoV-2: New Treatment Option for COVID-19. *Antimicrob Agents Chemother* **64** (2020).

17 Hoffmann, M. *et al*. SARS-CoV-2 Cell Entry Depends on ACE2 and TMPRSS2 and Is Blocked by a Clinically Proven Protease Inhibitor. *Cell* **181**, 271-280 e278 (2020).

18 Riva, L. *et al*. Discovery of SARS-CoV-2 antiviral drugs through large-scale compound repurposing. *Nature* (2020).

19 Kang, Y. L. *et al*. Inhibition of PIKfyve kinase prevents infection by Zaire ebolavirus and SARS-CoV-2. *Proc Natl Acad Sci U S A* (2020).

20 Korber, B. *et al*. Tracking Changes in SARS-CoV-2 Spike: Evidence that D614G Increases Infectivity of the COVID-19 Virus. *Cell* **182**, 812-827 e819 (2020).

21 Yurkovetskiy, L. *et al*. Structural and Functional Analysis of the D614G SARS-CoV-2 Spike Protein Variant. *Cell* (2020).

22 Jiang, X. *et al*. Bimodular effects of D614G mutation on the spike glycoprotein of SARS-CoV-2 enhance protein processing, membrane fusion, and viral infectivity. *Signal Transduction and Targeted Therapy* **5** (2020).

23 Maisonnasse, P. *et al*. Hydroxychloroquine use against SARS-CoV-2 infection in non-human primates. *Nature* **585**, 584-587 (2020).

24 Lai, A. L., Millet, J. K., Daniel, S., Freed, J. H. & Whittaker, G. R. The SARS-CoV Fusion Peptide Forms an Extended Bipartite Fusion Platform that Perturbs Membrane Order in a Calcium-Dependent Manner. *J Mol Biol* **429**, 3875-3892 (2017).

25 Straus, M. R. *et al*. Ca(2+) Ions Promote Fusion of Middle East Respiratory Syndrome Coronavirus with Host Cells and Increase Infectivity. *J Virol* **94** (2020).

26 Low, A. M. *et al*. Plant alkaloids, tetrandrine and hernandezine, inhibit

calcium-depletion stimulated calcium entry in human and bovine endothelial cells. *Life Sci* **58**, 2327-2335 (1996).

27 Leung, Y. M., Berdik, M., Kwan, C. Y. & Loh, T. T. Effects of tetrandrine and closely related bis-benzylisoquinoline derivatives on cytosolic Ca2+ in human leukaemic HL-60 cells: a structure-activity relationship study. *Clin Exp Pharmacol Physiol* **23**, 653-659 (1996).

28 John P. Felix *et al.* Bis(benzylisoquinoline) Analogs of Tetrandrine Block L-Type Calcium Channels: Evidence for Interaction at the Diltiazem-Binding Site. *Biochemistry* (1992).

29 Anselmi, E. *et al.* Selective inhibition of calcium entry induced by benzylisoquinolines in rat smooth muscle. *J Pharm Pharmacol* **44**, 337-343 (1992).

30 Liu, Q. Y., Karpinski, E., Rao, M. R. & Pang, P. K. Tetrandrine: a novel calcium channel antagonist inhibits type I calcium channels in neuroblastoma cells. *Neuropharmacology* **30**, 1325-1331 (1991).

31 Ranganathan, S., Harmony, J. A. & Jackson, R. J. Effect of Ca2+ blocking agents on the metabolism of low density lipoproteins in human skin fibroblasts. *Biochem Biophys Res Commun* **107**, 217-224 (1982).

32 Mori, S., Ito, H. & Yamamoto, K. Effects of calcium antagonists on low density lipoprotein metabolism in human arterial smooth muscle cells. *Tohoku J Exp Med* **154**, 329-333 (1988).

33 Daniloski, Z. *et al*. Identification of required host factors for SARS-CoV-2

infection in human cells. *Cell* (2020).

34 Tharappel, A. M., Samrat, S. K., Li, Z. & Li, H. Targeting Crucial Host Factors of SARS-CoV-2. *ACS Infect Dis* **6**, 2844-2865 (2020).

35 Xiu, S. *et al.* Inhibitors of SARS-CoV-2 Entry: Current and Future Opportunities. *J Med Chem* (2020).

36 Yang, L. *et al.* Identification of SARS-CoV-2 entry inhibitors among already approved drugs. *Acta Pharmacol Sin* (2020).

37 Yang, C. *et al.* Salvianolic acid C potently inhibits SARS-CoV-2 infection by blocking the formation of six-helix bundle core of spike protein. *Signal Transduct Target Ther* **5**, 220 (2020).

38 Wei, J. *et al.* Genome-wide CRISPR screens reveal host factors critical for SARS-CoV-2 infection. *Cell* (2020).

39 Danta, C. C. Calcium Channel Blockers: A Possible Potential Therapeutic Strategy for the Treatment of Alzheimer's Dementia Patients with SARS-CoV-2 Infection. *ACS Chem Neurosci* **11**, 2145-2148 (2020).

40 Kao, R. Y. *et al.* Identification of novel small-molecule inhibitors of severe acute respiratory syndrome-associated coronavirus by chemical genetics. *Chem Biol* **11**, 1293-1299 (2004).

41 Wang, N. *et al.* Structure of MERS-CoV spike receptor-binding domain complexed with human receptor DPP4. *Cell Res* **23**, 986-993 (2013).

42 Lu, G. *et al.* Molecular basis of binding between novel human coronavirus MERS-CoV and its receptor CD26. *Nature* **500**, 227-231 (2013).

43 Nathan, L. *et al.* Calcium Ions Directly Interact with the Ebola Virus Fusion Peptide To Promote Structure-Function Changes That Enhance Infection. *ACS Infect Dis* **6**, 250-260 (2020).

44 Das, D. K. *et al.* Conformational changes in the Ebola virus membrane fusion machine induced by pH, Ca2+, and receptor binding. *PLoS Biol* **18**, e3000626 (2020).

45 Gunaratne, G. S., Yang, Y., Li, F., Walseth, T. F. & Marchant, J. S. NAADP-dependent Ca2+ signaling regulates Middle East respiratory syndrome-coronavirus pseudovirus translocation through the endolysosomal system. *Cell Calcium* **75**, 30-41 (2018).

46 Straus, M. R., Bidon, M., Tang, T., Whittaker, G. R. & Daniel, S. FDA approved calcium channel blockers inhibit SARS-CoV-2 infectivity in epithelial lung cells. *Biorxiv* (2020).

47 Hu, J. *et al.* Development of cell-based pseudovirus entry assay to identify potential viral entry inhibitors and neutralizing antibodies against SARS-CoV-2. *Genes Dis* (2020).

48 Niesen, F. H., Berglund, H. & Vedadi, M. The use of differential scanning fluorimetry to detect ligand interactions that promote protein stability. *Nat Protoc* **2**, 2212-2221 (2007).

Figure legends

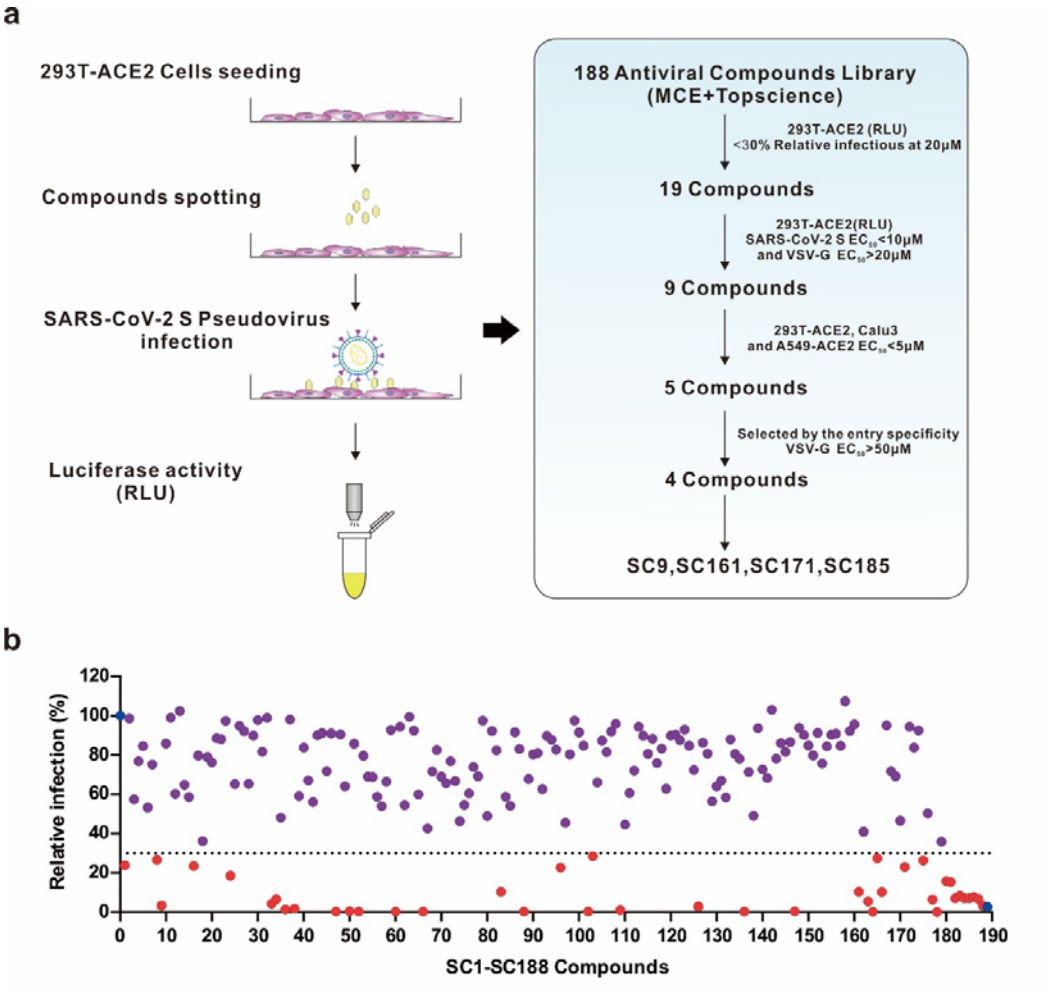

Fig. 1 Screening of compounds active against SARS-CoV-2 S-G614 pseudovirus in 293T-ACE2 cells. a Schematic diagram of the screening method and workflow. The screening method is shown on the left, and the selection criteria for hits are outlined on the right side. **b** Scatter plot of primary screening of 188 compounds against S-G614 infection. Inhibition ratios for all drugs obtained in a preliminary screening are represented by scattered points. Red dots indicate the 41 compounds with an inhibition rate ≥70%. DMSO and E-64d were used as a negative and positive control, respectively.

607

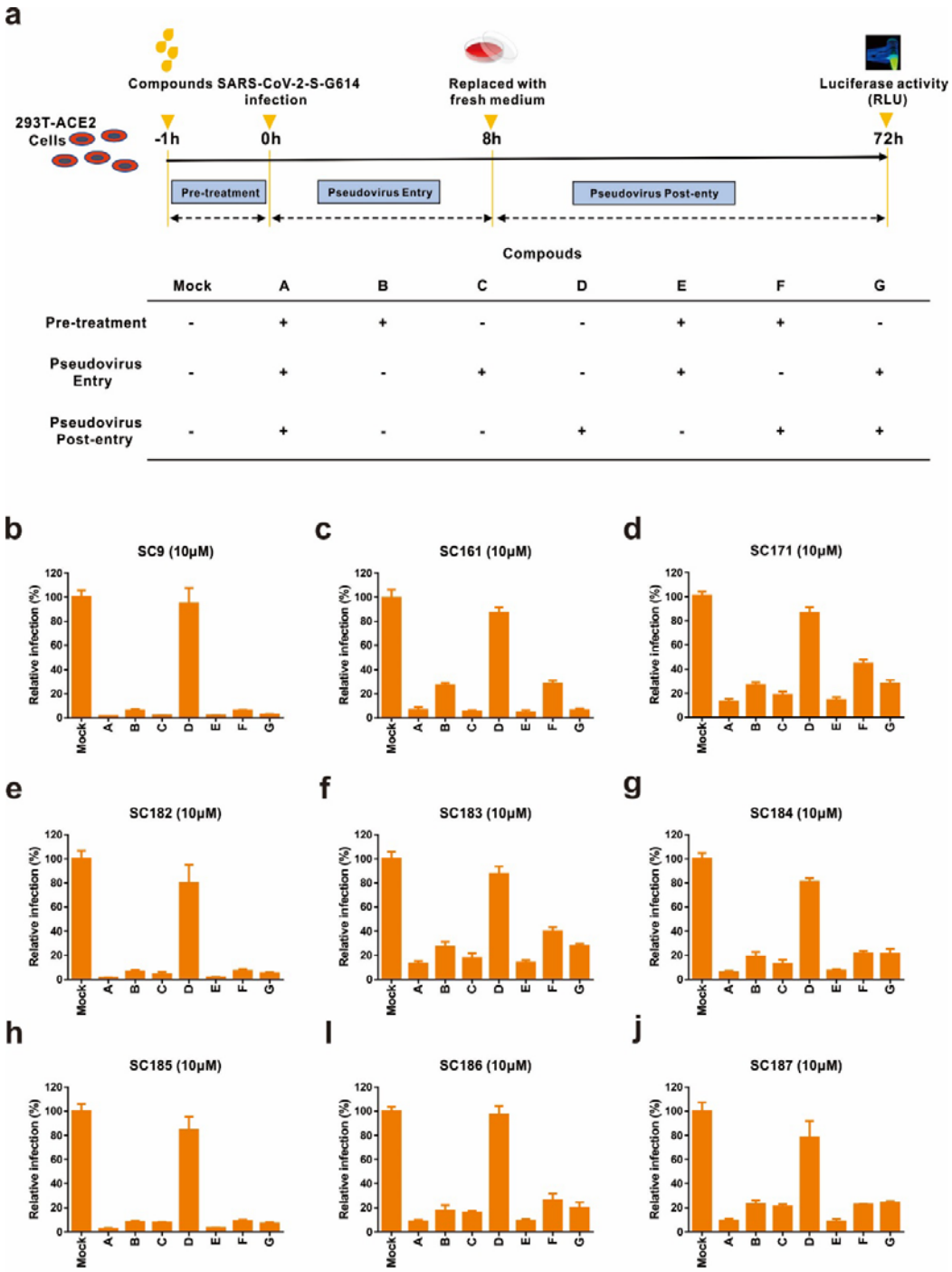

Fig. 2 Effect of treatment timing on the efficacy of nine selected compounds on SARS-CoV-2 S-G614 pseudovirus entry. a Treatment timing diagrams for the nine selected compounds. HEK 293T cells were treated with the nine compounds or DMSO before, during, or after S-G614 pseudovirus entry. Eight treatment conditions

(A–G) were tested for each compound. **b–j** Inhibitory effects of **(b)** SC9, **(c)** SC161, **(d)** SC171, **(e)** SC182, **(f)** SC183, **(g)** SC184, **(h)** SC185, **(i)** SC186, and **(j)** SC187 on the entry of S-G614 pseudovirus at different treatment time points. All experiments were repeated at least three times.

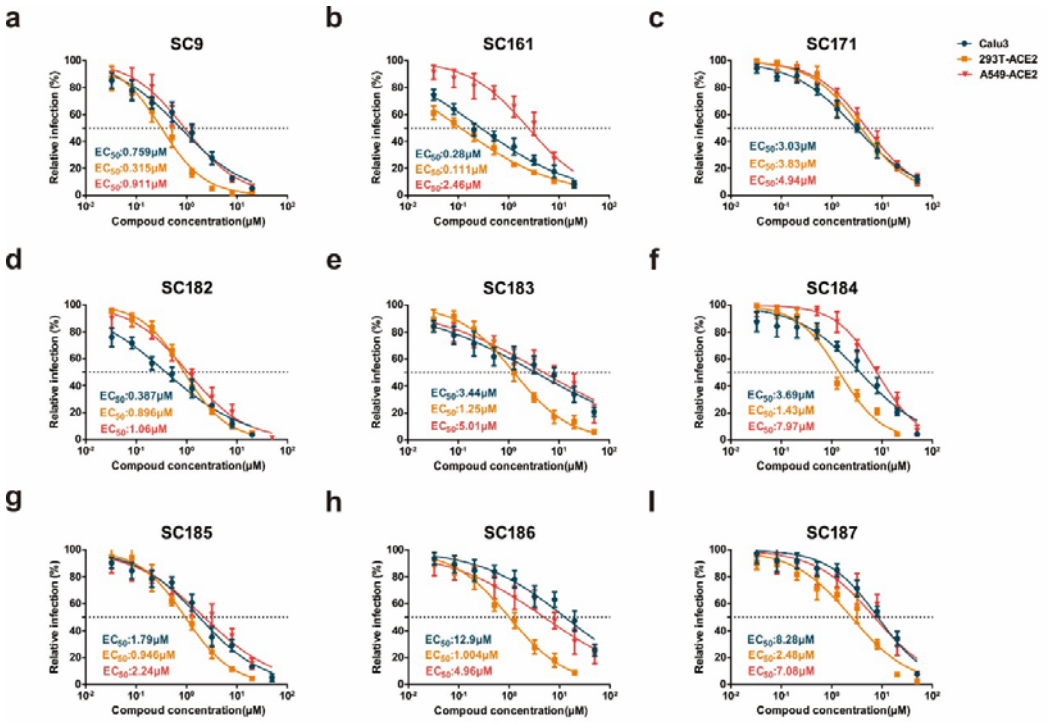

Fig. 3 Efficacy of nine compounds in Calu3, 293T-ACE2, and A549 cell lines. Inhibitory effects of **(a)** SC9, **(b)** SC161, **(c)** SC171, **(d)** SC182, **(e)** SC183, **(f)** SC184, **(g)** SC185, **(h)** SC186, and **(i)** SC187 against S-G614 infection in the three cell lines. All experiments were repeated at least three times.

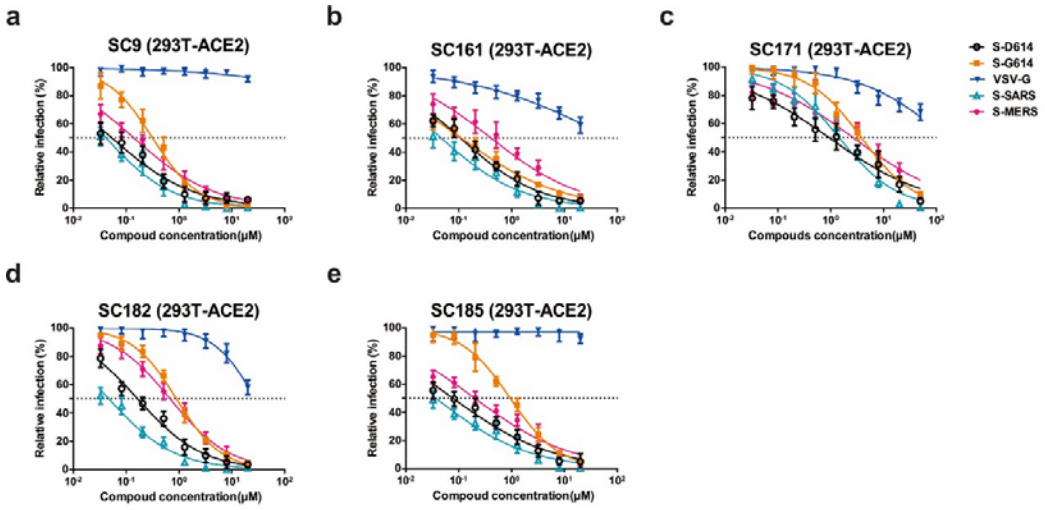

f

Compounds	S-D614	S-G614	VSV-G	S-SARS	S-MERS
	EC_{50}(μM)				
SC9	0.0537	0.315	>50	0.0417	0.140
SC161	0.107	0.111	>50	0.0464	0.409
SC171	0.932	3.83	>50	1.45	2.68
SC182	0.165	0.896	27.87	0.0472	0.681
SC185	0.078	0.946	>50	0.0372	0.202

Fig. 4 Dose-response curves for five broad-spectrum inhibitors of five types of coronaviruses. a–e Inhibition curves of five selected compounds **(a)** SC9, **(b)** SC161, **(c)** SC171, **(d)** SC182, **(e)** SC185 on S-D614, S-G614, S-SARS, S-MERS, and VSV-G pseudoviruses. **f** EC_{50} values of five selected compounds against entry of different pseudoviruses. All experiments were repeated at least three times.

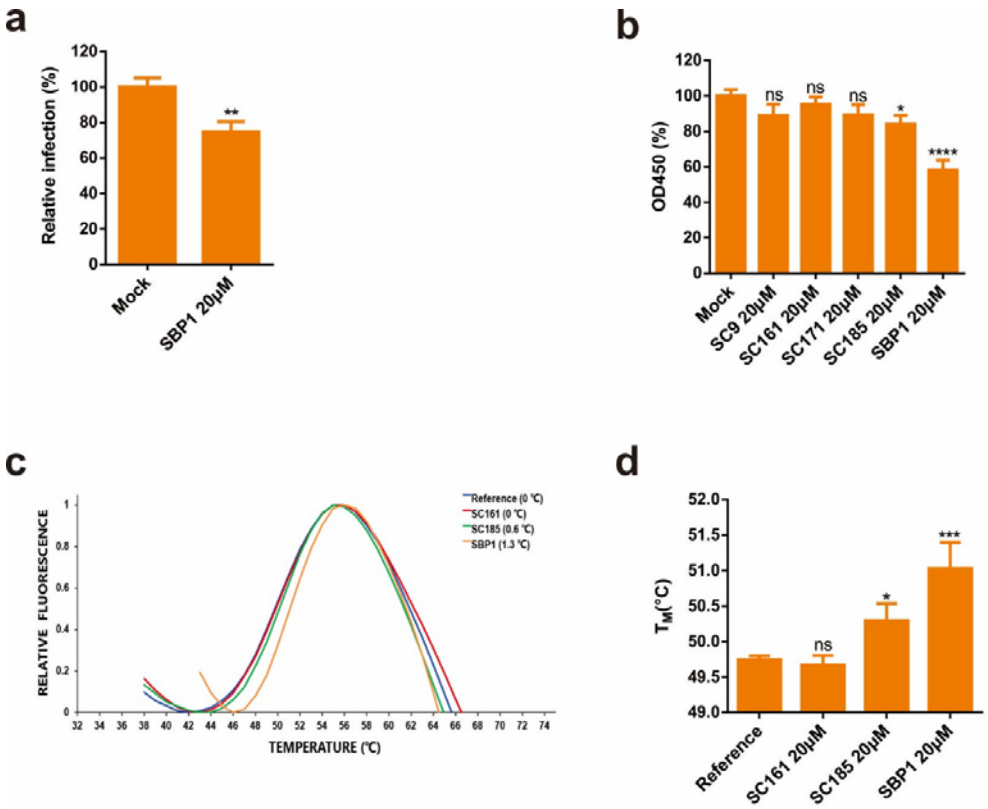

Fig. 5 Interactions between four selected compounds and the SARS-CoV-2 RBD domain. a Inhibitory effect of the ACE2 peptide SBP1 at 20 μM on the invasion of S-G614 pseudovirus. **b** Binding of pre-coated His-RBD with compounds at 20 μM as determined by competitive ELISA. SBP1 and DMSO were used as a positive and negative control, respectively. **c** Melting curves for His-RBD (10 μM) incubated with 20 μM of each compound tested by differential scanning fluorimetry. **d** T_M values of His-RBD incubated with SC161, SC185, or SBP1. All experiments were repeated at least three times.

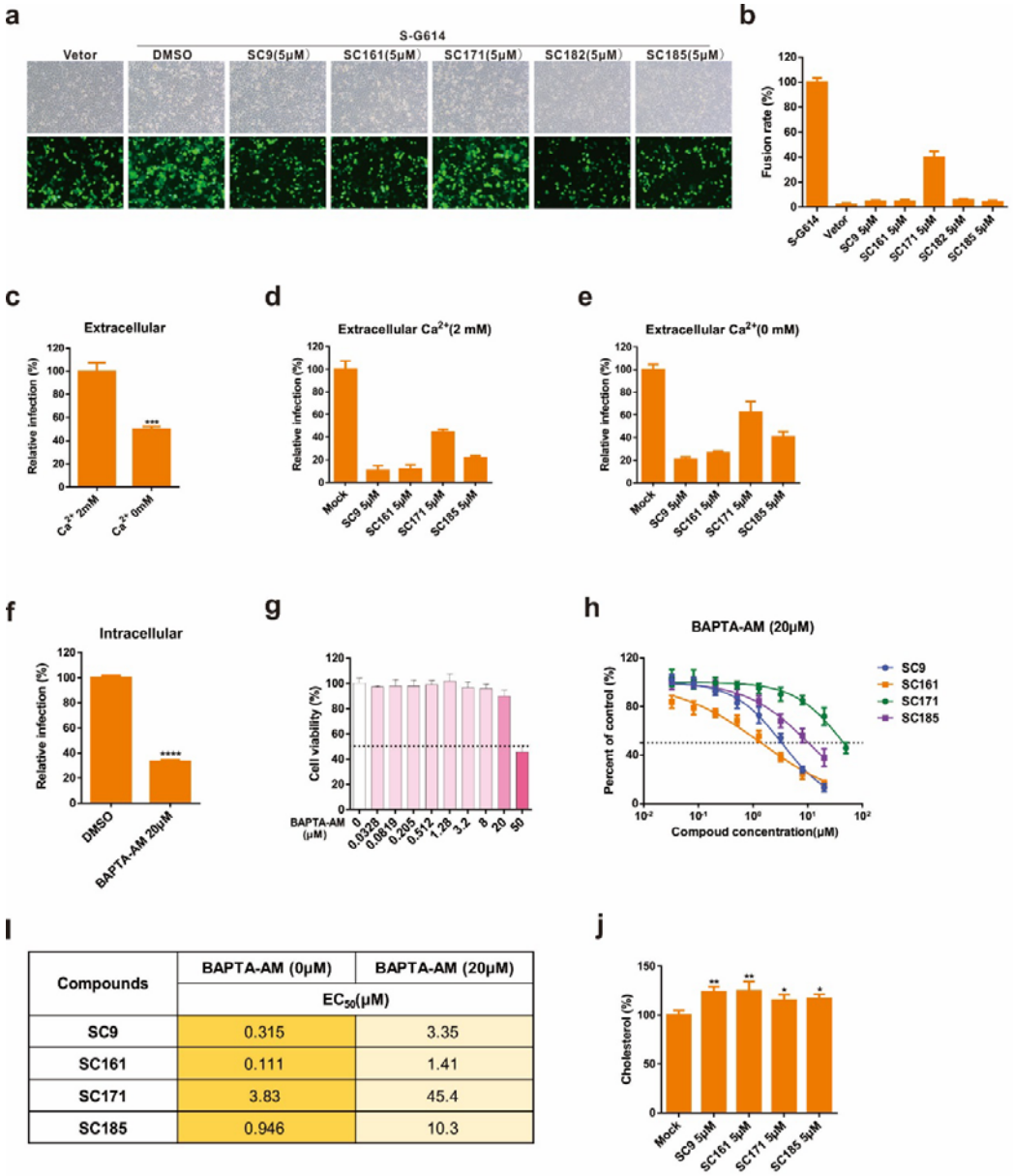

I

Compounds	BAPTA-AM (0μM)	BAPTA-AM (20μM)
	EC_{50}(μM)	
SC9	0.315	3.35
SC161	0.111	1.41
SC171	3.83	45.4
SC185	0.946	10.3

Fig. 6 Investigation of the mechanism of the selected compounds. a Inhibitory effect of SC9, SC161, SC171, SC182, and SC185 at 5 μM on SARS-CoV-2 S mediated cell-cell fusion. **b** Cell–cell fusion rate in the presence of 5 μM SC9, SC161, SC171, SC182, or SC185. The fusion rate in a DMSO-treated group was set as 100%. **c** Effect of extracellular Ca^{2+} depletion on S-G614 pseudovirus entry. **d** Effect of 5 μM of each compound on S-G614 pseudovirus entry into 293T-ACE2 cells in medium

supplemented with 2 mM $CaCl_2$. **e** Effect of 5 μM of each compound on S-G614 pseudovirus entry in calcium-depleted culture medium. **f** Effect of intracellular Ca^{2+} depletion using 20 μM BAPTA-AM on S-G614 pseudovirus entry. DMSO was used as a control. **g** Cell viability assay of 293T-ACE2 cells treated with increasing concentrations of BAPTA-AM (0–50 μM). **h** Inhibition curves of the compounds against S-G614 pseudovirus entry in the presence of 20 μM BAPTA-AM. **i** EC_{50} values of the compounds for S-G614 pseudovirus entry in the presence or absence of 20 μM BAPTA-AM. **j** Cholesterol (normalized to total protein) in 293T-ACE2 cells treated with the compounds or DMSO for 24 h. All experiments were repeated at least three times.

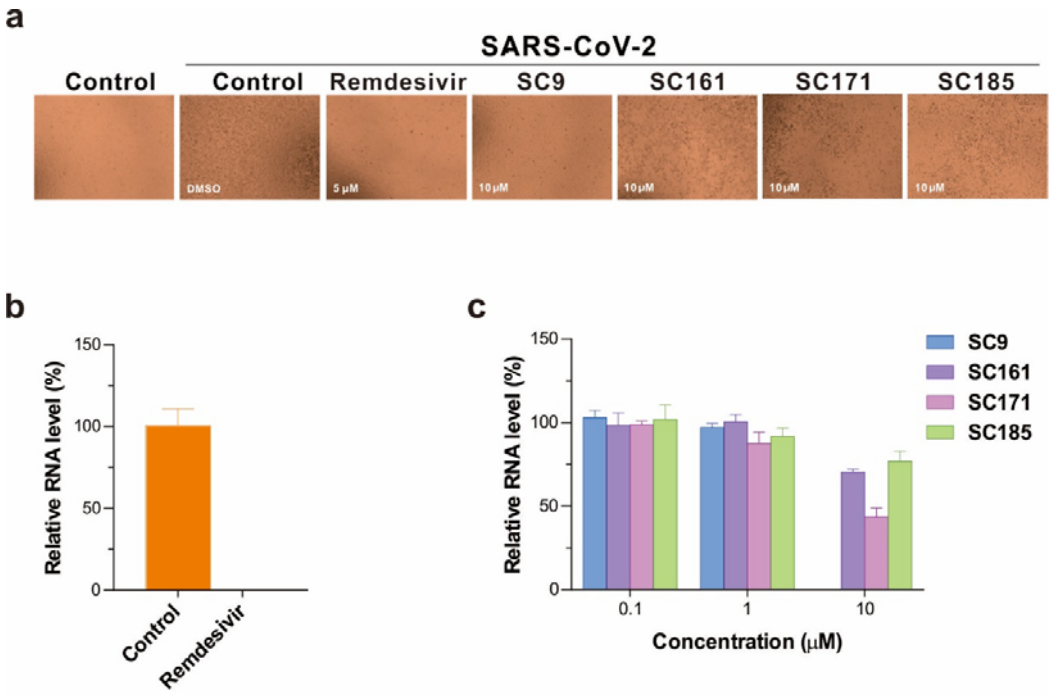

Fig. 7 Antiviral activities of four selected compounds against authentic SARS-CoV-2 in Vero E6 cells. a We assessed the inhibitory effect of the compounds on native SARS-CoV-2 infection by observing their cytopathogenic effects. SC9, SC161, SC171, and SC185 were tested at 0.1 μM, 1 μM, 10 μM, and DMSO and remdesivir (5 μM) were used as a negative and positive control, respectively. **b** The relative RNA level in the DMSO treatment group was set to 100%, and that in the positive control remdesivir (5 μM) treatment group was 0.01%. **c** The relative RNA levels in the SC9, SC161, SC171, and SC185 (10 μM) treatment groups were 70.27%, 43.55%, 76.98% and 0.08%, respectively. At 1 and 0.1 μM, relative RNA levels did not significantly decrease. All experiments were repeated at least three times.